

## **BOLTED RHS END-PLATE JOINTS IN AXIAL TENSION**

Fredrik Torp Karlsen<sup>a</sup> and Arne Aalberg<sup>b</sup>

<sup>a</sup> *Department of Structural Engineering, NTNU / Hjertnes ByggRådgivning AS, NO-3211 Sandefjord, Norway*

<sup>b</sup> *Department of Structural Engineering, NTNU, Rich. Birkelandsvei 1a, NO-7491 Trondheim, Norway*

**Abstract:** An experimental study is carried out for end-plate joints for rectangular hollow sections (RHS) in axial tension. Two designs of the plate are considered; one with bolts on two opposite sides of the RHS, and one with bolts on all four sides. The objectives are to determine how well the yield line mechanisms model the capacity and how the stiffness of the joint is predicted by the component method. Supplementary finite element simulations of the tests are added to support the discussion. Results show that the failure mechanisms assumed in EN 1993-1-8 for extended end-plates can be identified in the laboratory tests, and they yields quite reasonable predictions of the capacity. The initial elastic stiffness of the joints is overestimated if the standard T-stub analogy is applied; therefore a modified approach is suggested.

### **1 Introduction**

EN 1993-1-8 [1] presents rules for the calculation of the capacity and stiffness of joints based on the component method. Here, connection elements such as plates and bolts are characterized by their basic mechanical properties in tension, compression, bending or shear. The rules are mainly applicable for members of H- and I-profile and for commonly used joint design. For other joint designs or for joints between members of other structural shapes, the effects of the loading and the behaviour of the connection components must be considered in each particular case.

Bolted joints with end-plates are commonly used for joints connected on the building site. Rules for such joints for rectangular hollow sections are not explicitly covered by the EN 1993 part 1-8, as the design provisions of its chapter 6 are given for elements of H- or I-sections, while chapter 7, for hollow section, only treats welded joints in trusses.

The bolted end-plate connection for rectangular hollow sections (RHS) comprises bolts, end-plate and welds between the plate and the hollow section. The weld is typically a fillet weld, continuous around the section. The end-plate may extend outside the section on two opposite sides (Fig. 1), or on all four sides (Fig. 6).

Extended end-plate connections for RHS-sections and for H- and I-sections are quite similar, as illustrated in Fig. 1. The bolts are normally placed in one line (one row), and as close as possible to the section wall to minimize the bending moment in the end-plate, and to limit the increase in bolt force due to the level arm effect. For H-and I-sections, which have most of their cross-sectional area and force in the flanges, it is common to use bolts on both the out-

side and inside of the flange. Welds are placed on both sides of the flange and web. This provides a centric load transfer from the section walls to the end-plate, as assumed in the T-stub model commonly used.

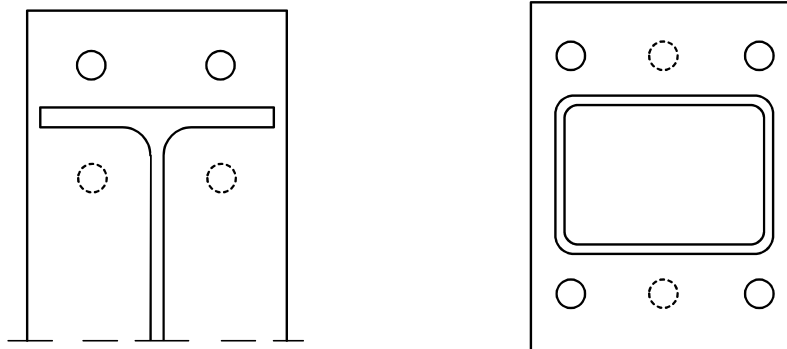


**Fig. 1:** End-plate connection for I-beam and RHS section.

For RHS end-plate joints, the weld is placed along the outside periphery of the section, where also the bolts have to be placed, leading to an unavoidable eccentricity. With bolts on two sides of the RHS the axial force of the entire section will have to be transmitted primarily through the two adjacent section walls. Furthermore, there is a rectangular “unsupported” part of the end-plate inside the section. Depending on the position of the bolts along the RHS wall, and the relationship between the thicknesses of the end-plate and the RHS wall, the part of the end-plate inside the section may be subjected to significant bending. This bending causes both bending and axial deformation of the RHS walls, most prominent in the parts away from the corners. The FE illustration in Fig. 7 shows the RHS wall deformation. This causes a complication for the use of the T-stub model, and modifications may be needed for the T-stub formulas for plastic capacity of the end-plate, and for the component stiffness models.

The design of RHS end-plate joints bolted on two opposite sides is discussed in CIDECT [2], with reference to an investigation by Packer et al [3]. The main findings are that the full tensile capacity can be developed, and that there is a shift in the location of the hogging plastic line into the part of the end-plate inside the section. When writing the plastic work expression both the bending and the axial deformation of the section walls must be considered, and a design stress utilizing strain hardening in the end-plate should be introduced.

Kato and Mukai [4] and Willibald et al. [5 and 6] have considered axially loaded joints with end-plates bolted on four sides. The former proposed a complex yield line model based on various estimates of the prying force. The latter presented a more thorough analysis of the three-dimensional behaviour of the connection, discussed the representation by the T-stub model, and gave guidelines for positioning of the bolts. In [7] an investigation on bolted moment end-plate connection with eight bolts is presented, providing yield line models which easily may be modified to suit the present problem.

## 2 Models for capacity and stiffness

### 2.1 Capacity

Numerous investigations have shown that the T-stub model predicts the capacity of bolted joints quite accurately. Using the notation of EN 1993-1-8 three failure modes must be considered:

i) Complete yielding of the flange of the T-stub 
$$F_{T,1,Rd} = \frac{4M_{pl,1,Rd}}{m} \quad (1)$$

ii) Failure of the bolts combined with yielding of the flange 
$$F_{T,2,Rd} = \frac{2M_{pl,2,Rd} + n \sum F_{t,Rd}}{m + n} \quad (2)$$

iii) Failure of the bolts alone 
$$F_{T,3,Rd} = \sum F_{t,Rd} \quad (3)$$

The capacity depends on the effective length  $l_{eff}$  of the equivalent T-stub used to represent the parts of the connection, which enters the equations through the plastic moment  $M_{pl}$ . The formulas for  $l_{eff}$  in EN 1993-1-8 are derived from considerations of the plastic mechanism in the end-plate, covering all relevant circular and non-circular yield line patterns. Examples of such patterns are shown in Fig. 2, both for individual bolts and for bolt groups. As the yield line method is based on the upper-bound theorem of the plasticity theory, the capacity may be non-conservative. Hence it is necessary to check all possible yield line patterns, and identify the smallest  $l_{eff}$ . The relevant values for  $l_{eff}$  are shown in Table 1.

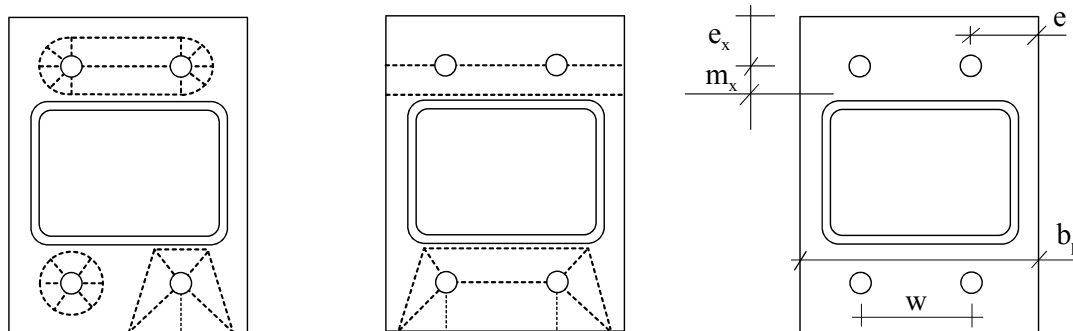


**Fig. 2:** Examples of circular and non-circular yield line patterns, and definition of geometry.

**Table 1:** Effective lengths for bolt row outside tension flange of section [1]

| Bolt row location                       | Bolt row considered individualley                             |   |
|---|---|---|
|   | Circular patterns<br>$l_{eff,cp}$                             | Non-circular patterns<br>$l_{eff,nc}$   |
| Bolt row outside tension flange of beam | Smallest of:<br>$2\pi m_x$<br>$\pi m_x + w$<br>$\pi m_x + 2e$ | Smallest of:<br>$4m_x + 1,25e_x$<br>$e + 2m_x + 0,625e_x$<br>$0,5b_p$<br>$0,5w + 2m_x + 0,625e_x$ |

Joints with bolts on all four sides of the section may also develop the basic yield line mechanisms around individual bolts and bolt groups (Fig. 2). In addition, one should consider more “global” yield line patterns extending around the RHS, as shown in Fig. 3. Also for this global type of yield mechanism it should be distinguished between cases with and without bolt failure, the latter causing more complex mechanisms and capacity formulas. Reference is made to [4] for cases involving bolt failures, with separation of the plates at the bolt position. The examples in Fig. 3 both show failure in the end-plate, for which the plastic axial force easily may be determined.

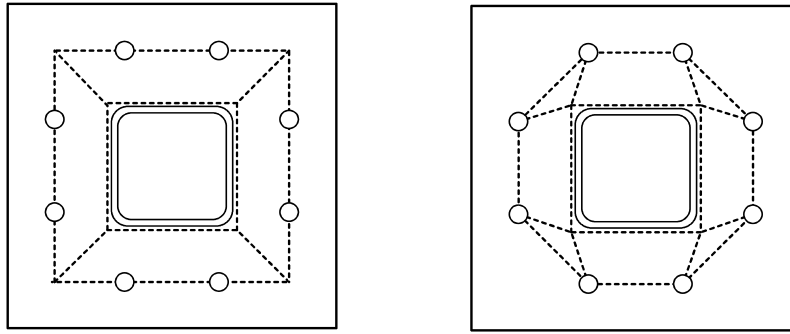


Fig. 3: Global yield line patterns in end-plate with bolts on four sides.

## 2.2 Stiffness model for T-stub

The axial flexibility of the joints is dominated by two contributions; bending of the end-plate and tensile deformation of the bolts. For end-plates welded to I- and H-sections, EN 1993-1-8 Table 6.11 introduces stiffness coefficients  $k_5$  and  $k_{10}$ , which are associated with plate bending and bolt elongation, respectively. The elastic deformation of the weld and axial straining of the section walls near the weld might contribute, but are not considered. These effects may be more prominent for RHS joints than for I- and H-joints.

The coefficients  $k_5$  and  $k_{10}$  were derived by Weynand, Jaspart and Steenhuis [8], using a model with a T-stub in bending, as shown in Fig. 4. The flange of the T-stub bends as a beam, supported by the bolts and the flange tips, the latter assumed to be contact points when lever arm deflections occur. The effective distance between the web of the tee and the bolt is  $m$ , and the distance between bolt and contact force  $Q$  is set equal to  $1,25m$ . An analysis determined the contact force to be  $Q=0,13F$  and bolt force equal  $0,63F$ . The subscripts are used as follows; p=plate, b=bolt.  $A_b$  is the bolt area and  $t_p$  is the plate thickness.

$$\text{End-plate in bending} \quad k_p = k_5 = \frac{0,9I_{eff}t_p^3}{m^3} \quad (4)$$

$$\text{Bolts in tension} \quad k_b = k_{10} = \frac{1,6A_b}{L_b} \quad (5)$$

The stiffness of the joint is determined by considering the two contributions as springs in a series:

$$k_{total} = \frac{1}{\frac{1}{k_p} + \frac{1}{k_b}} = \frac{1}{\frac{1}{k_5} + \frac{1}{k_{10}}} \quad (6)$$

Note that there are some unrealistic simplifications in the model, as the bending deformation of the flange between the contact point and the bolt location is physically impossible, Fig. 4 b. Furthermore, the deformation is assumed to remain unchanged when the elongation of the bolts is superimposed, Fig. 4 c. A more realistic model can be obtained by modelling the bolts as elastic supports.

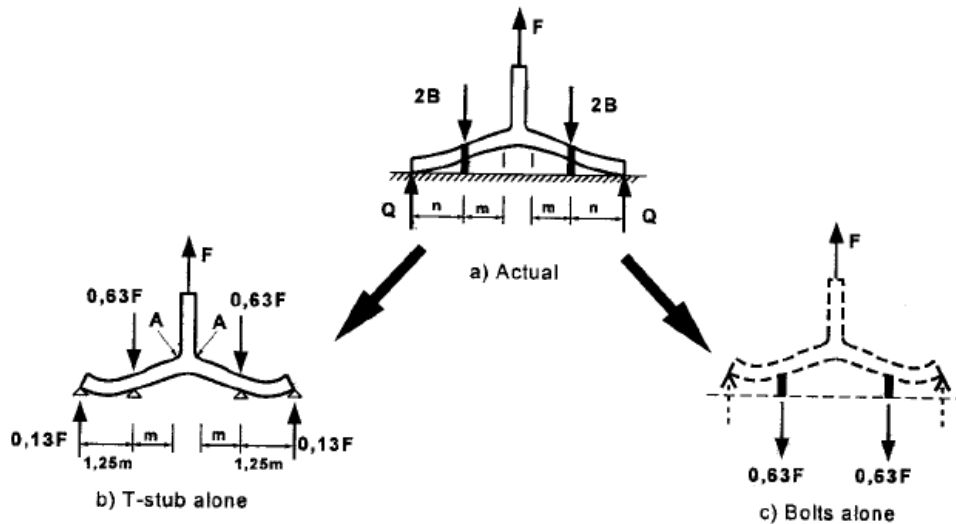


Fig. 4: Elastic deformation of T-stub model, from [8].

### 2.3 Stiffness model for RHS end-plate joint

The bending deformation of an end-plate in a RHS joint will differ from that shown above for the T-stub. The axial force in the member is transmitted to the end-plate through the welds, and is resisted by the bolt forces in the extended part of the end-plate. This results in a rotation of the plate at the junction with the section wall, and a vertical deflection of the plate within the section (Fig. 10). When establishing a conceptual model, advantage can be taken of the two symmetry lines in the plate. However, it should be noted that the deformation pattern is complex. The plate bends about two axes, and near the section corners the plate deformation is strongly restrained by the section geometry. Note also that the 2-D bending deformation will be more pronounced for joints with bolts along all four sides of the end-plate than for the case with bolts only on two sides.

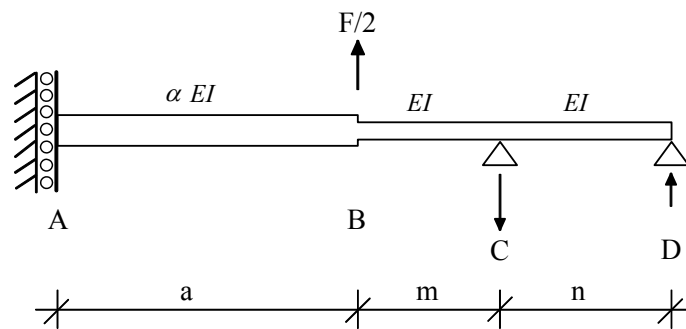


Fig. 5: Structural model for RHS end-plate in bending.

Fig. 5 shows a simple beam model proposed by for the determination of the stiffness coefficients  $k_p$  and  $k_b$ , Karlsten [9]. The model is one-dimensional, representing a beam strip of the end-plate, spanning from the symmetry line (point A) in the middle of the RHS to the free edge (point D) of the end-plate. For joints with bolts on two sides of the section the axial force  $F$  is carried by  $F/2$  by each of the walls adjacent to the bolts. The moment restraint from the RHS wall at point B is neglected. Due to the 2-D bending of the plate inside the section this part of the beam may be given an increased stiffness  $\alpha EI$ . The joint displacement is defined as that of point B.

Based on this model the stiffness coefficient for end-plate in bending  $k_p$  and for bolts in tension  $k_b$  can be derived as:

$$k_p = \frac{2(3a + 3m\alpha + n\alpha) \cdot l_{eff,ini} \cdot t_p^3}{m^2(3m^2\alpha + 4nm\alpha + 12am + 12an)} \quad (7)$$

and

$$k_b = \frac{4n(3a + 3m\alpha + n\alpha)}{(6am + 6an + 3m^2\alpha + 2n^2\alpha + 6nm\alpha)} \frac{A_b}{L_b} \quad (8)$$

### 3 Laboratory tests

#### 3.1 Test programme and procedure

A test program was carried out in order to provide data for the verification of the analytical models for joint stiffness and capacity. The section RHS 80·80·4 in S355 was chosen for all specimens. The end-plate was also in S355. Table 2 gives the test program and Fig. 6 shows the bolt locations.

Each test specimen was symmetrical, and consisted of two 500 mm long RHS members with end-plates connected by four or eight bolts, see Fig. 7. The specimens were manufactured by a commercial workshop, using ordinary tolerances and weld quality. The throat dimension varied between 3,5 and 4,0 mm. The bolts were fully threaded M16-grade 8.8 in holes 17 mm, and were tightened to 110 Nm. The welding introduced an initial curvature in the end-plate, which resulted in a significant initial gap at the plate edges when the two end-plates were connected. The chosen bolt pre-tensioning produced good contact between the end-plates in the region between the bolts, but a small gap remained at the edges.

Tensile tests of the end-plate materials were carried out. For  $t_p=8,0$  mm the values  $f_y = 464$  N/mm<sup>2</sup> and  $f_u = 590$  N/mm<sup>2</sup> were obtained, while for  $t_p=10,1$  mm the values were  $f_y = 360$  N/mm<sup>2</sup> and  $f_u = 530$  N/mm<sup>2</sup>.

The specimen tests were performed at a displacement rate of 1 mm/min in the elastic range, thereafter increased to 4 mm/min until failure, which occurred at displacements ranging from 12 to 25 mm. The load was measured with a 500 kN load cell in the test machine, and the displacement was measured at the grips. An accurate measurement of the joint displacement, i.e. the relative displacement between the two end-plates, was obtained by means of a digital image measuring (DIC) system.

**Table 2:** Test programme

| Test specimens | RHS (mm) | End-plate [mm] | Number of bolts |
|----------------|----------|----------------|-----------------|
| A1 and A2      | 80·80·4  | 8,0            | 4               |
| B1 and B2      | 80·80·4  | 10,1           | 4               |
| C1 and C2      | 80·80·4  | 8,0            | 8               |

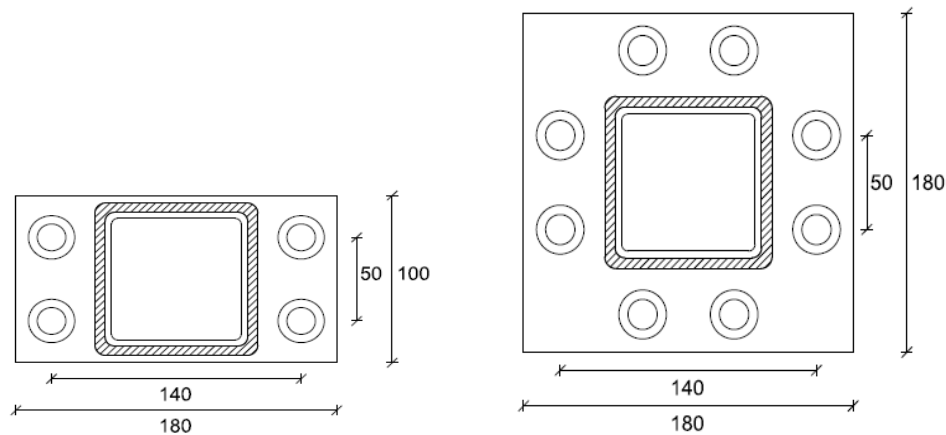


**Fig. 6:** Geometry of test specimen A and B (left), and C (right).

### 3.2 Test results

The experimental load-displacement curves are depicted in Figs. 8, 9 and 11. In addition, the response curves from the numerical simulation and the analytical models are included in the figures. The displacement is taken as the total displacement between the members, i.e. the opening between the plates, recorded by the digital image system. The two A-specimens (Fig. 8) softened significantly when the applied force reached approximately 170 kN. The tests were terminated at a displacement of 25 mm and a force of approximately 260 kN. Specimens B displayed the same type of response. For lack of space no curves for specimens B are presented here.

The two specimens C behaved differently from A and B, for obvious reasons. Fig. 11 shows the response curves. The end-plates are held together on all four sides by the bolts, the RHS pulled the end-plates in the region between the bolts, and no displacement occurs at the plate edges. The joint displacement is here based on monitoring two points on the RHS sidewall, adjacent to the weld, and approximately 32 mm apart. Due to the high strength of the 8 mm end-plate the failure in the tests is fracture of the weld, which for the weakest of the two specimens was as small as  $a=3$  mm. The axial yield force of the 80·80·4 RHS is 430 kN, which explains visible yielding also in the RHS in the tests. Permanent deformations in the end-plate (Fig. 12) comprises yielding along the welds, between the two bolts on each side, and yielding between bolts on neighbour sides, partly consistent with the yield line pattern as depicted to the right in Fig. 3. Again the RHS section walls are bent outwards near the end-plate. After the test, the end-plate has a permanent bow with amplitude approximately 8 mm.

## 4 Numerical model

Numerical simulations by means of Abaqus were performed for all specimens. Fig. 7 shows a section of the FE model for Specimens A. In order to simplify the model, the RHS members were modelled with 90 degrees corners, and only 200 mm of the RHS members were included in the model. The hexagonal head of the bolts was modelled as round, and the pre-tensioning was disregarded. The analyses were both geometrical and material nonlinear, using the stress-strain curves from the material tests. Since only pure tension was considered, symmetry in three planes ensured that only 1/8 of the physical specimen had to be modelled. Volume elements C3D8R, with nodes in all corners of the cubic element were used, all nodes having three translational degrees of freedom. The end-plates were meshed with four elements over

the thickness of the plate, while two elements were used for the RHS thickness. Surface to surface contact was used between bolt head and end-plate and between the end-plates, and the welds were modelled by the same element.

Fig. 7 shows a close-up photo of the A2 specimen, and the corresponding deformed shape obtained by the Abaqus simulation. The agreement is very good, both the end-plate, bolt shaft and RHS wall deformations are captured by the simulations.

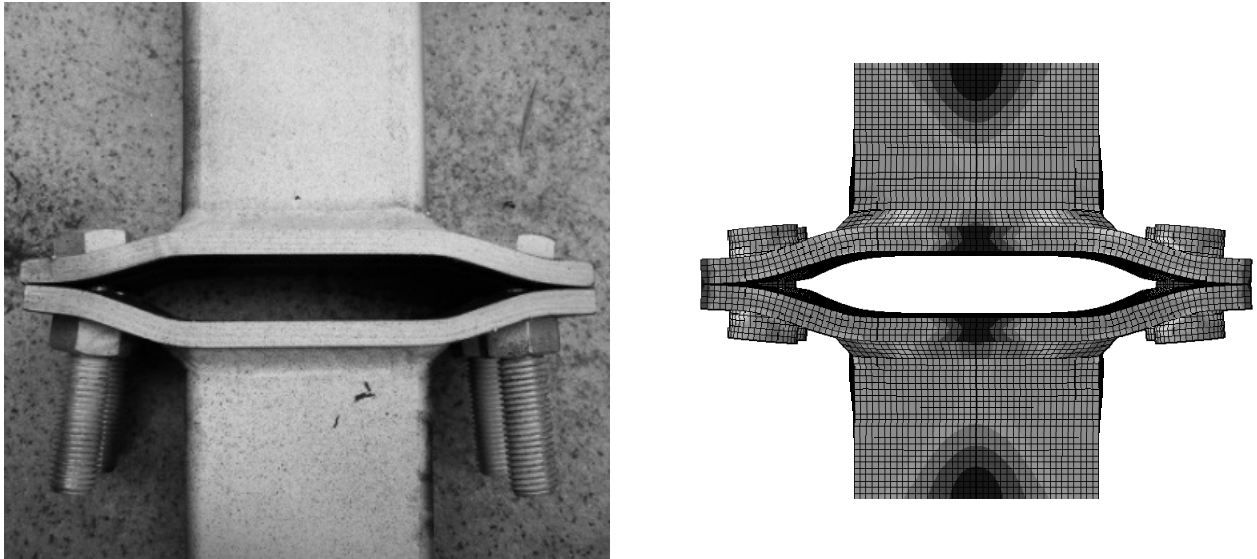


Fig. 7: Comparison of experimental and simulated deformation for Specimen A2.

## 5 Results and discussion of behaviour

### 5.1 Tests A

The response curves for Specimens A1 and A2, with bolts on two sides, are given in Fig. 8 for both experiments and Abaqus simulation.

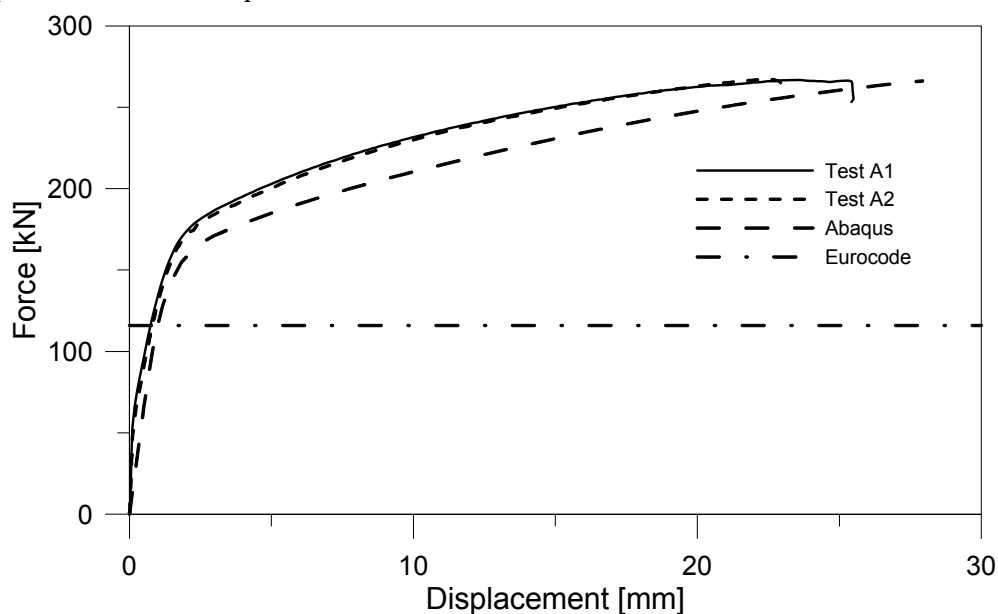
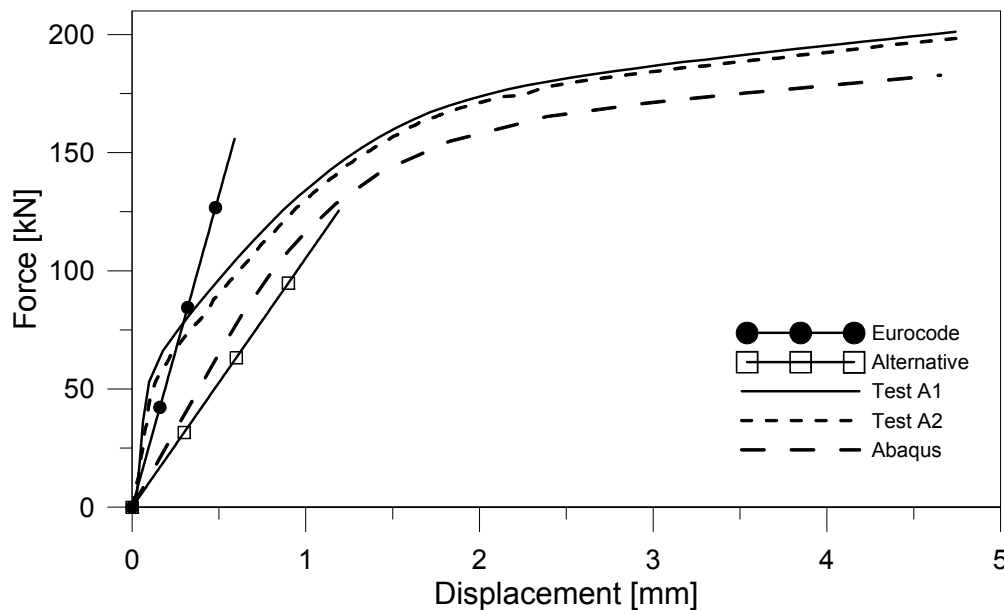


Fig. 8: Force-displacement curves for test specimens A1 and A2.

The displacement is taken as the relative displacement between the two end-plates. Measured values for geometry and material are used, without any material factor. The T-stub approach of Eurocode, with fully developed yielding in the end-plate (Eq. 1), gives a capacity of 116 kN, which is very much on the conservative side. Here, the non-circular pattern (Table 1) with T-stub length  $l_{eff,nc} = 0,5b_p$  on both sides of the RHS governs. The curve obtained from the Abaqus simulation lies only slightly below the test curves, and shows that the FE simulation may very well be used to predict and interpret tests on such components.



**Fig. 9:** Comparison of initial stiffness for specimens A1 and A2.

Fig. 9 shows a close-up of the initial part of the response curves given above. The straight lines in the graph represent the initial elastic stiffness calculated after Eurocode (Section 2.2) and the new alternative model outlined in Section 2.3, using the same effective length of the T-stub. As explained in [8], the effective length in stiffness calculations should be taken smaller than that determined from the yield line patterns. A length reduction corresponding to the elastic vs. plastic plate moment ratio ( $=2/3$ ) lead to the stiffness coefficient in Eq. 4. Following this concept, it can be shown [9] that  $l_{eff}$  for the alternative stiffness model should be replaced by  $l_{eff,ini}$  ( $=0,85 l_{eff}$ ), as done in Eq. 7. The bending stiffness of the end-plate inside the RHS is set equal to the stiffness in the extending parts in the computation of  $k_p$  and  $k_b$  in Eqs. 7 and 8, i.e.  $\alpha$  is here set to 1,0.

For both specimens the slope of the experimental curve is steep during the first 0.15 mm of displacement. This is caused by the pre-tensioning of the bolts, where the externally applied force primarily causes an unloading of the pre-compression between the end-plates, without any separation and/or bending. This has recently been studied in an experimental and numerical investigation [10], both with and without pre-tensioning of bolts, and end-plates with and without initial curvatures caused by welding (discussed in Section 3.1). The calculated stiffnesses are therefore not directly comparable with the tests.

The initial stiffness for the Abaqus simulation is perhaps a more realistic measure for a perfect test geometry. Comparing the calculated stiffnesses, with the Abaqus curve considered as the “correct” value, it is seen that the alternative model gives the best fit. We also see that com-

pared with the Abaqus result the Eurocode model overestimates the stiffness by a considerable margin, approximately 100 %.

Furthermore, the digital images show that separation of the plates initiates at a load somewhat higher than 50 kN. If the initial stiffness is read from the experimental curves at that load level we see that the agreement between the test and the alternative stiffness model is very good.

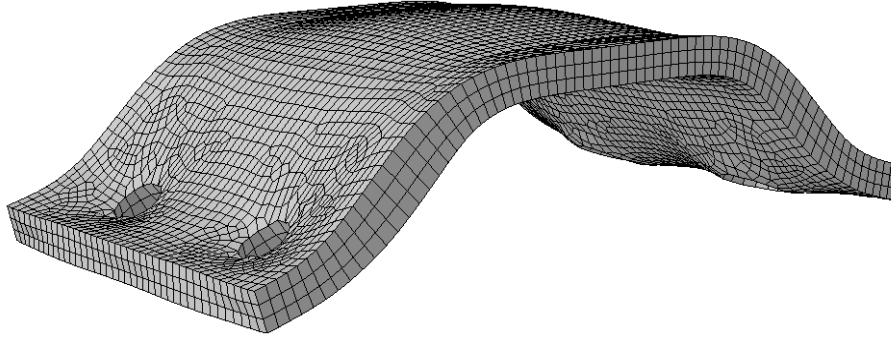


**Fig. 10:** Illustration of end-plate deformation (magnified) for specimen type A.

## 5.2 Tests B

Specimen B1 and B2 with  $t_p=10,1$  mm displayed the same type of response curves as Specimens A, with the same deformation of end-plates and RHS walls. Significant softening started at approximately 200 kN, and at 20 mm displacement the curve flattened out at force approximately 290 kN. The Eurocode capacity is again determined by failure mode 1 (Eq. 1), with predicted capacity 141 kN, which is about 40 to 50 % of the experimental value. The initial stiffness estimated with the alternative stiffness model is again close to the Abaqus simulation, and the Eurocode stiffness is far too high.

## 5.3 Tests C

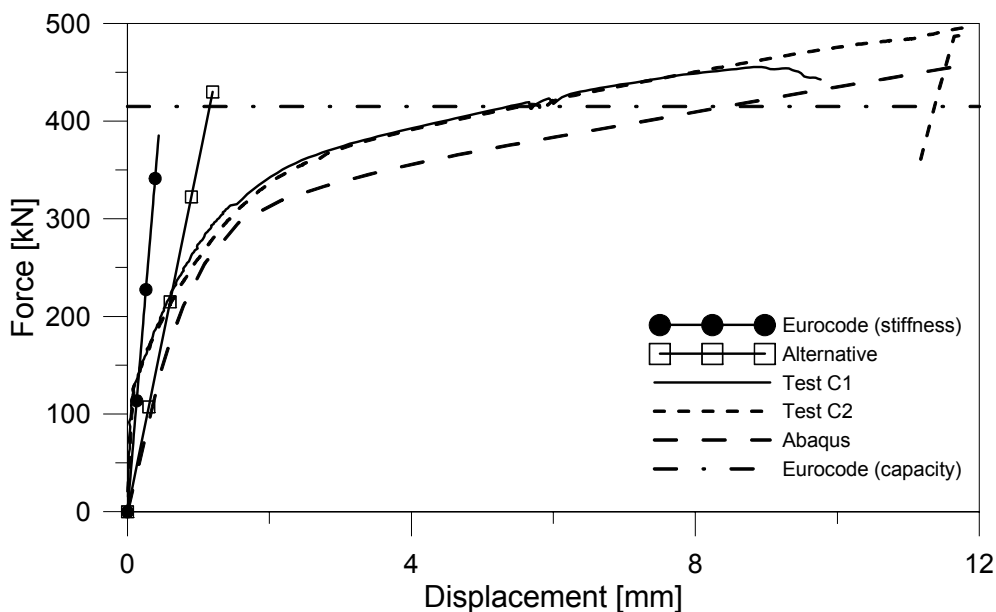


**Fig. 11:** Force-displacement curves and comparisons for specimens C1 and C2.

The response curves for Specimen C1 and C2 are shown in Fig. 11. Specimen C1 failed by fracture of the weld at a displacement of approximately 9 mm, while for Specimen C2 the test was terminated when the capacity of the test machine (and the RHS) was reached. These specimens are significantly stronger than the others, due to the increased number of bolts and the increased stiffness of the end-plate assembly. Fig. 12 shows yield marks on the deformed end-plate of Specimen C2, symmetrical around the section.

The capacity according to the T-stub model of Eurocode is for this geometry 415 kN, as indicated in Fig. 11. However, in this case the global yield line mechanisms shown in Fig. 3 determine, giving a capacity of approximately 325 kN, which agrees quite well with the stiffness degradation of the specimens, i.e. the knee of the curves. The Abaqus curve shows a reasonable agreement with the tests.

For the calculation the axial stiffness the same plate strip is used (Fig. 5), but in this case the force in the section wall is only  $F/4$ . As shown in the figure, this gives a stiffness prediction quite similar to that of the Abaqus simulation.

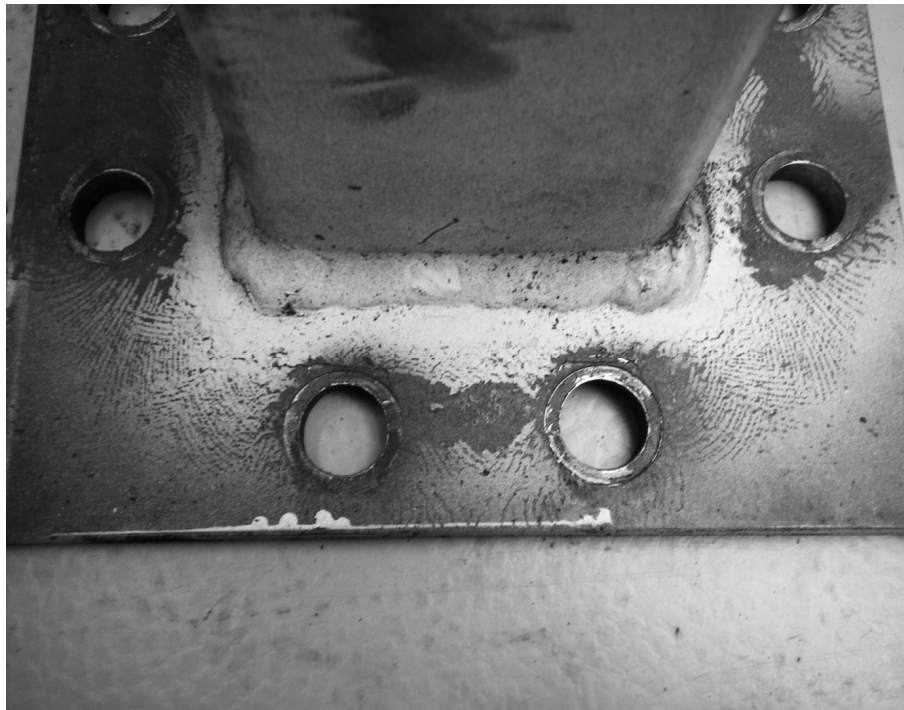


**Fig. 12:** Yield-pattern in end-plate of test specimen C2.

## 6 Conclusions

For specimens with bolts on two sides of the RHS the failure mechanism in the end-plates is the same as predicted by the T-stub model of Eurocode; i.e. complete yielding of the flange plate. There is a large margin of safety in the calculated capacity. For the specimens with bolts on all four sides of the RHS the yield mechanisms go around the section, and additional yield line models must be applied. The numerical FE simulations show good agreement with the response of the specimens, in particular for the inelastic behaviour. The stiffness in the initial part of the experimental response curves is affected by the bolt pre-tension. The stiffness models based on beam analogy are therefore compared with the stiffness in the simulations, where the geometry of the end-plate is modelled with perfect (flat) geometry. Use of the

stiffness coefficients of Eurocode for the RHS end-plate specimens produces too high stiffness values, whereas the suggested alternative stiffness model shows promising results.

## References

- [1] EN 1993-1-8:2005, Eurocode 3: “Design of steel structures - Part 1-8: Design of joints”, CEN, 2005.
- [2] CIDECT, “Design guide for rectangular hollow section (RHS) joints under predominantly static loading”, *CIDECT* 2009.
- [3] Packer J.A., Bruno L. and Birkemoe P.C. “Limit analysis of bolted RHS flange plate joints”. *Journal of Structural Engineering*, Vol. 115, No.9, 1989.
- [4] Kato B. and Mukai A., “Bolted tension flanges joining square hollow section members”, *Journal of Constructional Steel Research*, Vol. 5, Issue 3, pp. 163-177, 1985.
- [5] Willibald S., Packer J.A. and Puthli R.S., “Experimental study of bolted HSS flange-plate connections in axial tension”, *Journal of Structural Engineering*, American Society of Civil Engineers, Vol. 128, No. 3, pp. 328-336, 2002.
- [6] Willibald S., Packer J.A. and Puthli R.S., “Design recommendations for bolted rectangular HSS flange-plate connections in axial tension”, *Engineering Journal*, American Institute of Steel Construction, Vol. 40, First Quarter, pp. 15-24, 2003.
- [7] Wheeler A., Clarke M. and Hancock G.J., “Design model for bolted moment end plate connections joining rectangular hollow section using eight bolts”, Research report No R827, Department of Civil Engineering, The University of Sydney, 2003.
- [8] Weynand K., Jaspart J.P., Steenhuis M. “The stiffness model of revised annex J of Eurocode 3”, *Proceedings of the 3rd International Workshop on Connections* (Eds.: R. Bjorhovde, A. Colson, R. Zandonini), Trento, Itália, 441-452, 1995.
- [9] Karlsen F.T., “Knutepunkter for staver med hulprofiltverrsnitt – Joints for elements of hollow sections” (in Norwegian), Master thesis, Department of Structural Engineering, Norwegian University of Science and Technology (NTNU), June 2011.
- [10] Ersland, H., “Endplateskjöt for hulprofiler – End plate joints for hollow sections” (in Norwegian), Master thesis, Department of Structural Engineering, Norwegian University of Science and Technology (NTNU), December 2011.